Chapter 4

Carbon Films from Camphoric Carbon Soot Target by Pulsed Laser Deposition

4.1 Introduction

Nowadays, various methods are used for the preparation of carbon films [1-6]. In fact, the energy of the carbon species generated by various preparation methods is different and plays an important role in controlling the sp^3/sp^2 ratio. In the past decade, pulsed laser deposition (PLD) process has become popular for its ability to generate highly energetic carbon species [7] which enhances the formation of high percentage of sp^3 bonded carbon atoms at low substrate temperatures, and therefore, deposition of high quality of DLC film can be realized. In spite of adequate distinct advantages, the low deposition rate hinders commercialization and restricts the PLD process to the sophisticated research areas only.

Graphite is being used almost exclusively as the target material for physical vapor deposition of DLC films systems, such as, sputtering [4], filtered cathodic vacuum arc (FCVA) [6], PLD [8] etc. Therefore, additional hydrogen gas/ ions are needed to get hydrogenated carbon where hydrogen is used to passivate the dangling bonds in the gap states and also to tailor the optoelectronic properties [1] for a specific application. However, camphoric carbon (CC) soot obtained from burning camphor (($C_{10}H_{16}O$), a natural source, might be a new precursor material and has hydrogen abundantly in its structure. Furthermore, the presence of sp^3-hybridized bonds in camphor molecule might play an beneficial role for the deposition of carbon films.

In this chapter, we present the deposition of DLC films from camphoric carbon target (CCT) by PLD, and compare the results with those of DLC films obtained from conventional graphite target (GT) in search of new target material with more desirable performance. The deposited films are examined by Raman, optical absorption, SEM microscopy, AFM image and ESR spectroscopic investigations.

4.2 Experimental Details
4.2.1 PLD Deposition System

DLC films were deposited on silicon and quartz substrates by excimer laser (NISSIN 10X, XeCl, λ = 308 nm, τ = 20 nsec, repetition rate = 2 Hz, spot size = 5.5 mm^2), which is focused on the target at an incident angle of 45° to the target normal. The deposition system has a stainless steel high vacuum chamber that is evacuated by a turbomolecular pump. The schematic of the deposition chamber is shown in Fig. 4.1. The substrate was mounted parallel to the target at a distance of 45 mm. The films were deposited at room temperature at a base pressure of 10^{-6} Torr. The laser pulse energy was 150 mJ on the window.

4.2.2 Precursor

Details of the chemical structure of the starting precursor camphor, the camphor burning system and the target preparation method have been described in the previous chapter. In brief, camphor was burnt in a quartz tube and the soot deposited along the walls of the tube was collected, dried in the oven for about 1 hour and pressed into pellets in order to use them as targets in PLD. For comparison, commercial graphite target was used. The deposition parameters were kept the same for the two targets. The films deposited on quartz substrates were used for Raman, optical absorption and ESR analyses.

4.2.3   Thickness Measurement and Comparison

The thickness of the deposited films is measured by Alpha-Step 500 profiler. Deposition rate is found to be 0.05 and 1.45 Å on quartz and 0.13 and 1.5 Å per pulse on silicon substrates for graphite and CC targets, respectively. The rates of deposition on quartz and silicon very different for graphite, while it is almost the same for camphoric carbon target. Moreover, the deposition rate of camphoric carbon target is about 10 and 30 times higher than the graphite on silicon and quartz substrates, respectively.
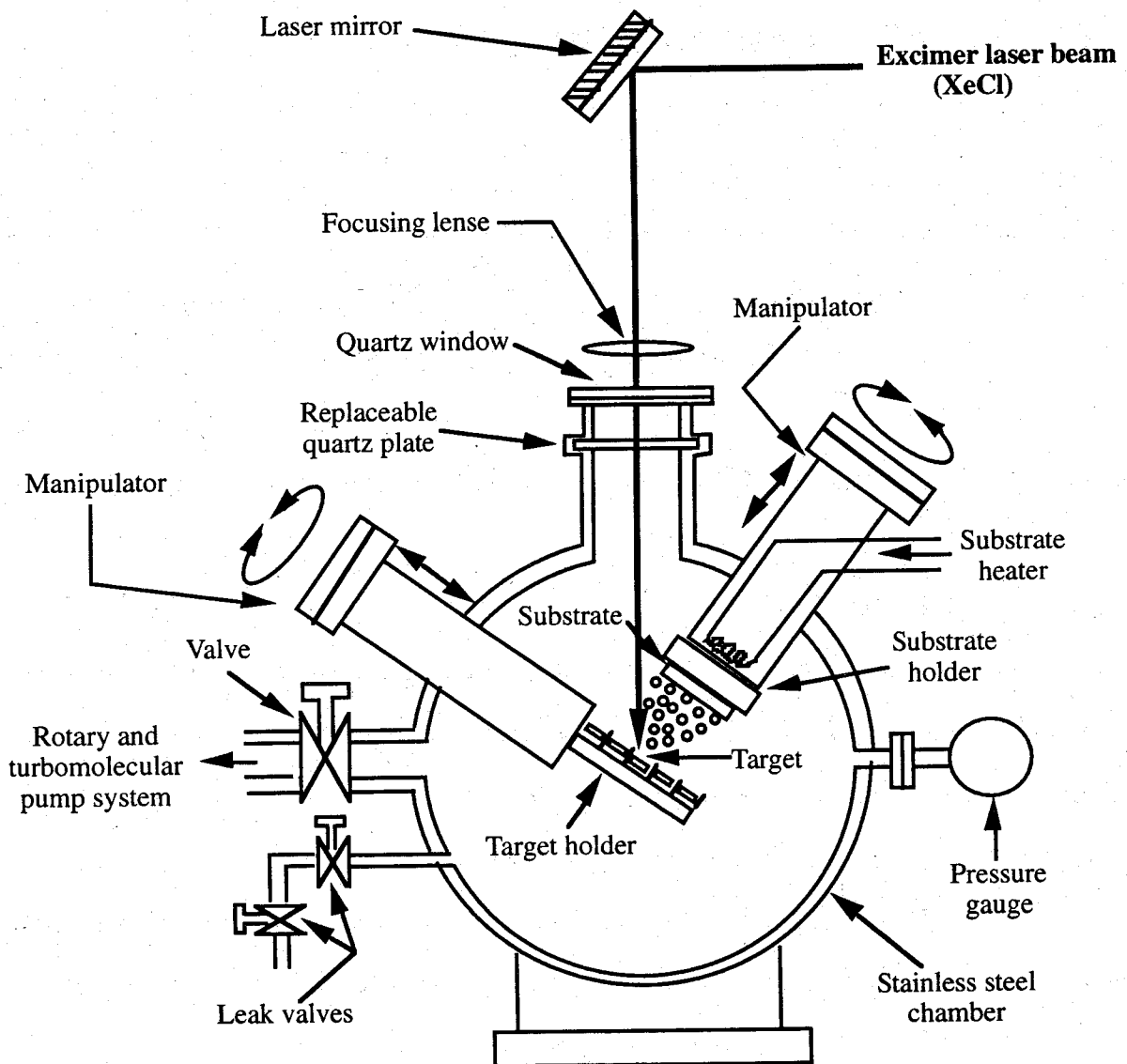
Figure 4.1. Schematic of the pulsed laser deposition chamber

4.3 Results and Discussions

4.3.1. Structural Properties

4.3.1.1 Raman Spectroscopy

The first order Raman spectra (RS) consist of a single sharp line at about 1332 cm^{-1} for diamond and 1580 cm^{-1} (G line) for single crystal graphite. The G line results from the Raman allowed E_{2g} mode, while another line appears at about 1350 cm^{-1} (D line) for polycrystalline graphite due to grain boundary effect [9]. RS were obtained in the quasi-backscattering geometry using 488 nm line of Ar$^+$ ion laser. Figure 4.2 shows the RS of the camphoric carbon (CC) and graphitic carbon (GC) thin films and their corresponding targets.
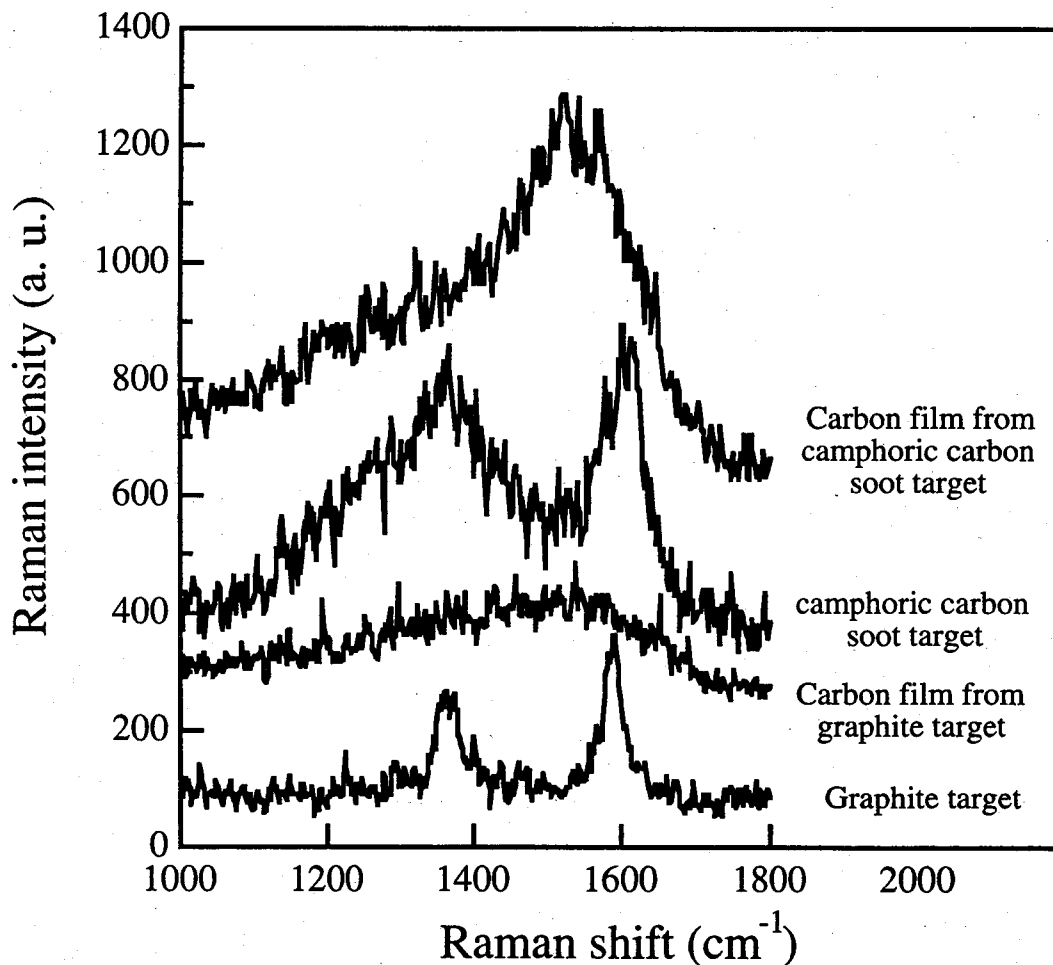
Figure 4.2. Raman spectra of camphoric and graphitic carbon films and their respective targets.

The spectra are vertically displaced for clarity, but otherwise displayed using the same scale. The RS of the CC film exhibits typical DLC structure [10] and the spectra of the GC film is different and similar to the amorphous carbon [11-13] (less diamond-like structure). In order to evaluate the structural features, the experimental data are best fitted by two Gaussian lines and the fitting parameters are listed in Table 4.1.

TABLE 4.1: Raman fitting parameters for camphoric and graphitic carbon films and their respective targets.

Samples	D - line position (cm⁻¹)	G - line position (cm⁻¹)	D – linewidth (FWHM) (cm⁻¹)	G - linewidth (FWHM) (cm⁻¹)	I_D/I_G
Camphoric carbon target	1358	1605	366	73	4.8
Camphoric carbon film	1356	1545	388	175	1.2
Graphite target	1365	1587	48	37	0.9
Graphitic carbon film	1364	1550	440	225	2.1

The downshift of G line from graphitic position (~1580 cm⁻¹) has confirmed the presence of both sp³ and sp² hybridized bonds [14] and disordered structure [15] in these laser deposited films. Both D and G Raman linewidths and integrated intensity ratio (I_D/I_G) of the D line to the G line are smaller in CC film, which indicate lesser disorder [14, 16] in CC

film. When compared with the targets, position of the G line of the films is observed to have downshifted while D line remains unchanged. On the other hand, the G and D linewidths of GC films are observed to increase about 6 and 9 times, respectively, whereas for the CC film, only the G linewidth is doubled and D linewidth remains unaltered, which reflect the presence of a large amount of disorder in the GC film. However, compared to CCT, Raman linewidths (FWHM) are much smaller in GT, showing presence of less disorder in the latter. Furthermore, the G line position at about 1605 cm^{-1} clearly indicates presence of highly disordered bonded carbon atoms [16] in CCTs. Very interestingly, the disorder in CC film is less while its target is highly disordered compared to graphite target. Moreover, Raman peak intensity of the CC film is much higher (thickness of the films is almost the same) which confirms the structural differences between the films. Resonance Raman effect, which was related to difference of trihedral bonding (π) and antibonding (π^*) states [17], might be responsible for this phenomenon.

4.3.2   Optical Properties

4.3.2.1   Optical Absorption and Tauc Gap

Figure 4.3 shows the optical absorption spectra of the films obtained from optical transmittance and reflectance measurements in the range of 200 to 2000 nm. The high absorption in the power-law (Tauc) and exponential (Urbach) region is ascribed to the presence of more graphitic component (sp^2 bonds) in the GC film. Puretzky et al. [18] reported DLC films from graphite target using ArF (193 nm) and KrF (248 nm) laser beams, where the film obtained from the shorter wavelength laser had better diamond-like properties. The optical absorption spectra in this experiment have a similar shape to the absorption spectra reported by Puretzky et al. [18]. The absorption nature of CC film can be compared to that of the film obtained from ArF laser while for GC film it can be compared to that from KrF laser. The optical gap, E_{opt} is obtained from the extrapolation of the linear part of the curve at the absorption coefficient $\alpha=0$ (in the inset of Fig. 4.3) using the Tauc relation [19],

$(\alpha h v)^{1/2} = B(E_{opt} - h v)$, where, B is the Tauc parameter. The estimated E_{opt} and B parameter are about 0.9 eV and 320 $(cm\text{-}eV)^{-1/2}$ for CC while 0.5 eV and 250 $(cm\text{-}eV)^{-1/2}$ for GC films, respectively.
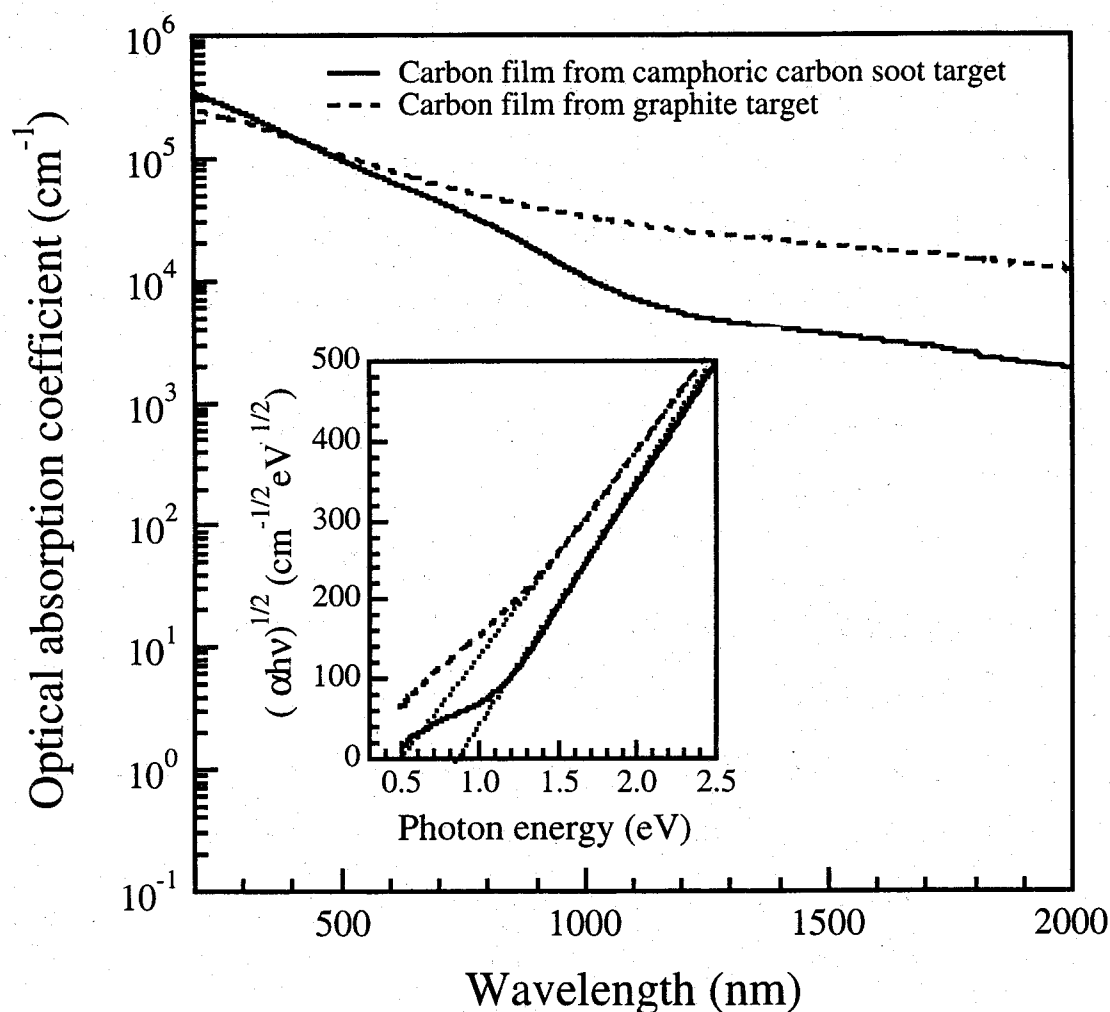
Figure 4.3. Optical absorption coefficient (α) plotted as a function of photon energy (hv), for camphoric and graphitic carbon films. The inset shows plot of $(\alpha h v)^{1/2}$ as a function of hv for the same samples.

4.3.3　Optical Gap and Raman Parameters Correlation

The optical gap, which can be correlated with the I_D/I_G [20], is higher while I_D/I_G ratio is smaller (Table 4.1) in CC film and is in good agreement with the correlation. The larger optical gap reveals more diamond-like nature and hence more sp^3 bonded structure.

4.3.4　Gap States

The B value in the CC film is reasonably high compared to the earlier reported value [21]. ESR spectroscopy is used to measure density of defect states and are estimated to be 1.8 $\times 10^{20}$ and $6 \times 10^{20} cm^{-3}$ for CC and GC films, respectively.

Physical processes that control the behavior of gap states in non-crystalline semiconductors are structural disorder responsible for the tail states and structural defects in deep states [22]. The Tauc parameter, B, is a measure of the steepness of band tail (Urbach region) density of states [23]. Higher value in CC film is due to less structural disorder [24], agreeing with Raman analysis of these films. Further, lower spin density reveals less defects in the deep states.

4.3.5　Surface Morphology and Structure

4.3.5.1　Scanning Electron Microscopy

Figure 4.4 shows scanning electron microscope (SEM) image of the carbonaceous films deposited from graphite (Fig. 4.4(a)) and camphoric carbon (Fig. 4.4(b)-(c)) targets. Surface morphology reveals strong dependency on their respective targets. In the case of GC film, the grain size is so small that it is not understandable from the graph of 200 K magnification, whereas, ball-like grain size having diameter of about 100~250nm is observed for the CC film. This much big grain size is unusual feature for the carbonaceous film deposited at room temperature, However, this phenomenon observed to occur [25] for the films deposited/heat treated at high temperatures due to the a) formation and agglomaration of graphitic crystallites b) conversion of sp^3 carbon to sp^2 carbon in the film thereby becoming
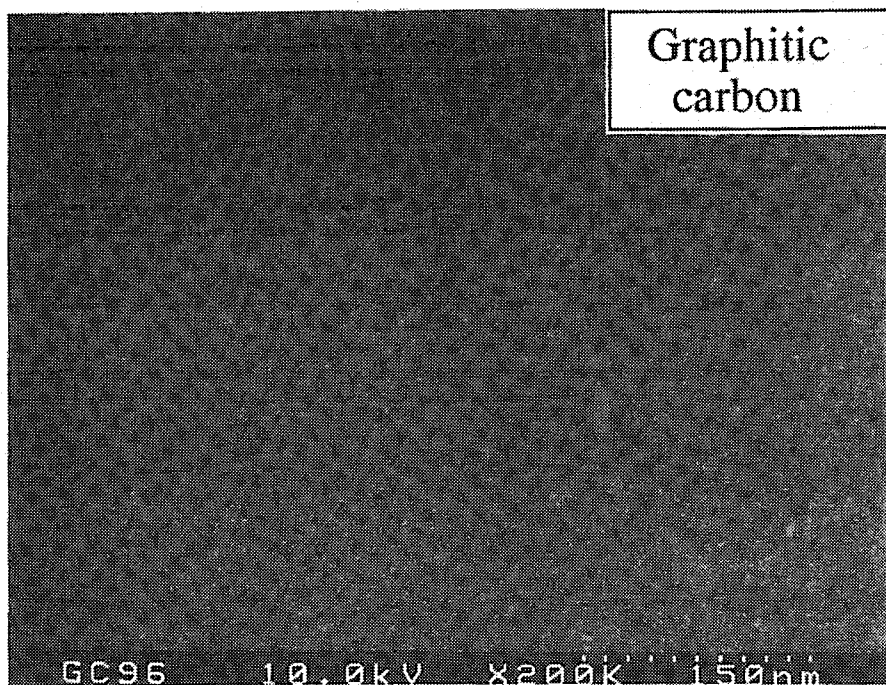
Figure 4.4a.   Scanning electron micrograph image of carbon film obtained from graphite

target (200,000 times magnification).
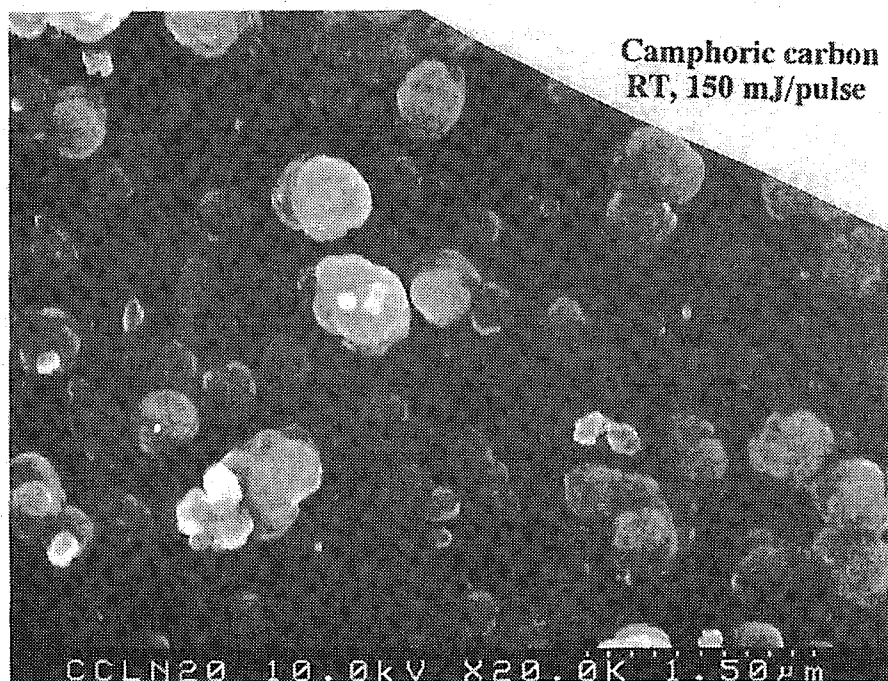
Figure 4.4b. Scanning electron micrograph image of carbon film obtained from camphoric

carbon target (20,000 magnification).
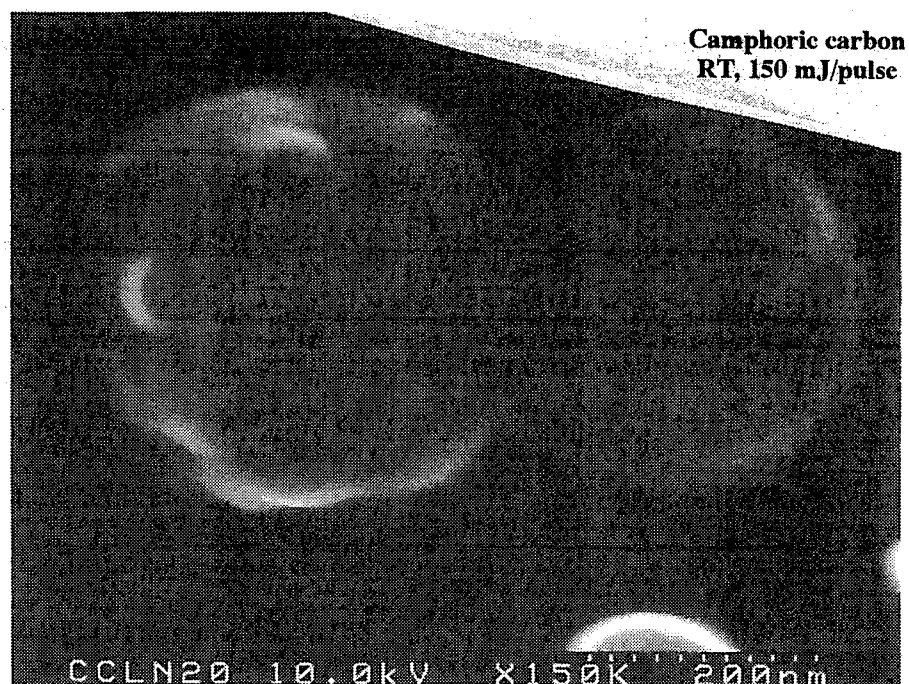
Figure 4.4c. Scanning electron micrograph image of carbon film obtained from camphoric carbon target (150,000 magnification).

more graphitelike. But interestingly, the CC film possesses higher sp^3 bonded carbon in its structure indicates this phenomena might be due to role of hydrogen/ oxygen present in the precursor material.

4.3.5.2   Atomic Force Microscopy

Atomic force microscopy (AFM) image of the carbon films obtained from graphite and camphoric carbon soot targets are shown in Figs. 4.5a and 4.5b, respectively and agrees well with the SEM image shown in Fig. 4.4.

4.3.6   Growth Kinetics of CC Film

However, in addition to graphite, there have been efforts to obtain carbonaceous films using a few other solid targets, such as glassy carbon [26] and phenol resin [27]. It has been observed that these films have less diamond-like properties compared to the films obtained from graphite target. In fact, the formation of DLC films by PLD is believed to be an ion

assisted energetic condensation process where the kinetic energy of the carbon species is one of the most important factors that affect the film properties. The energy of the carbon species ablated from graphite and CC targets is expected to be different because of the different bonding environments [28]. In light of the earlier observations for glassy carbon and graphite targets [24] and comparing our results, we speculate that the kinetic energy of the species of CC would be higher than that from graphite [29]. The higher kinetic energy then could help the formation of better quality DLC film that we have obtained from CC targets.
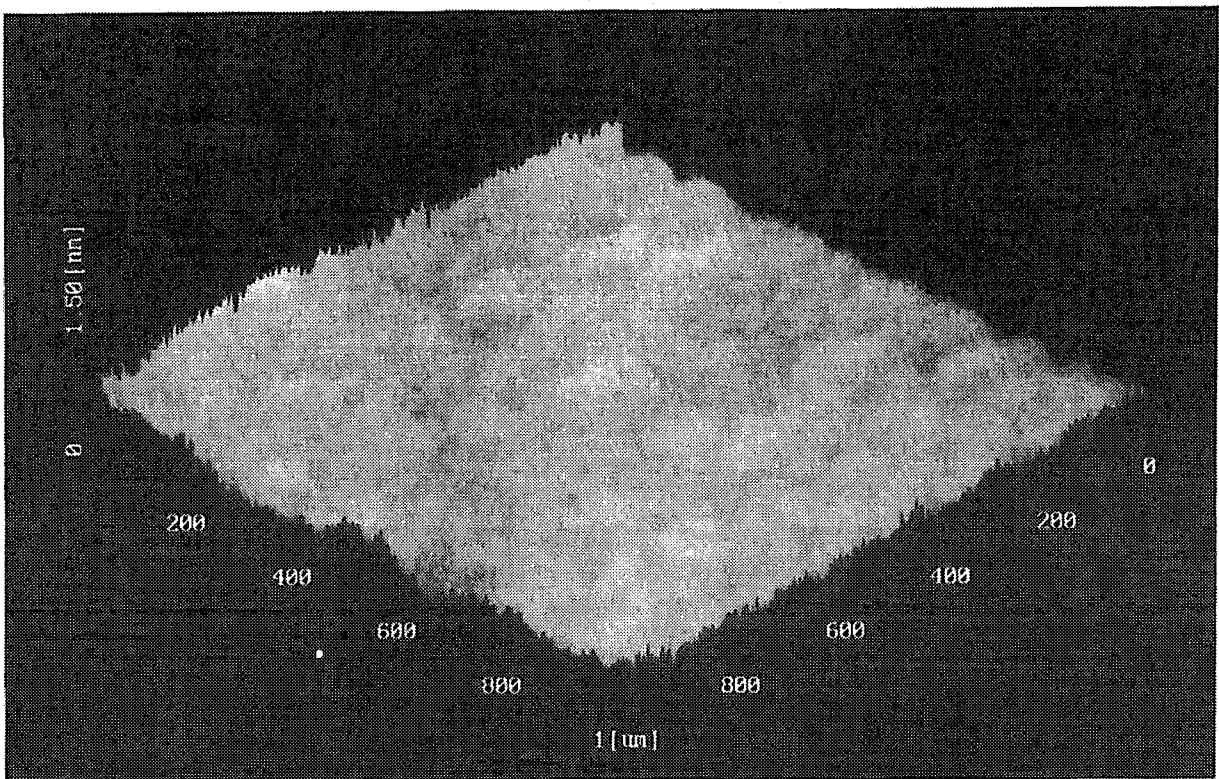
Figure 4.5a. Atomic force microscopy (AFM) image of carbon film obtained from graphite target.
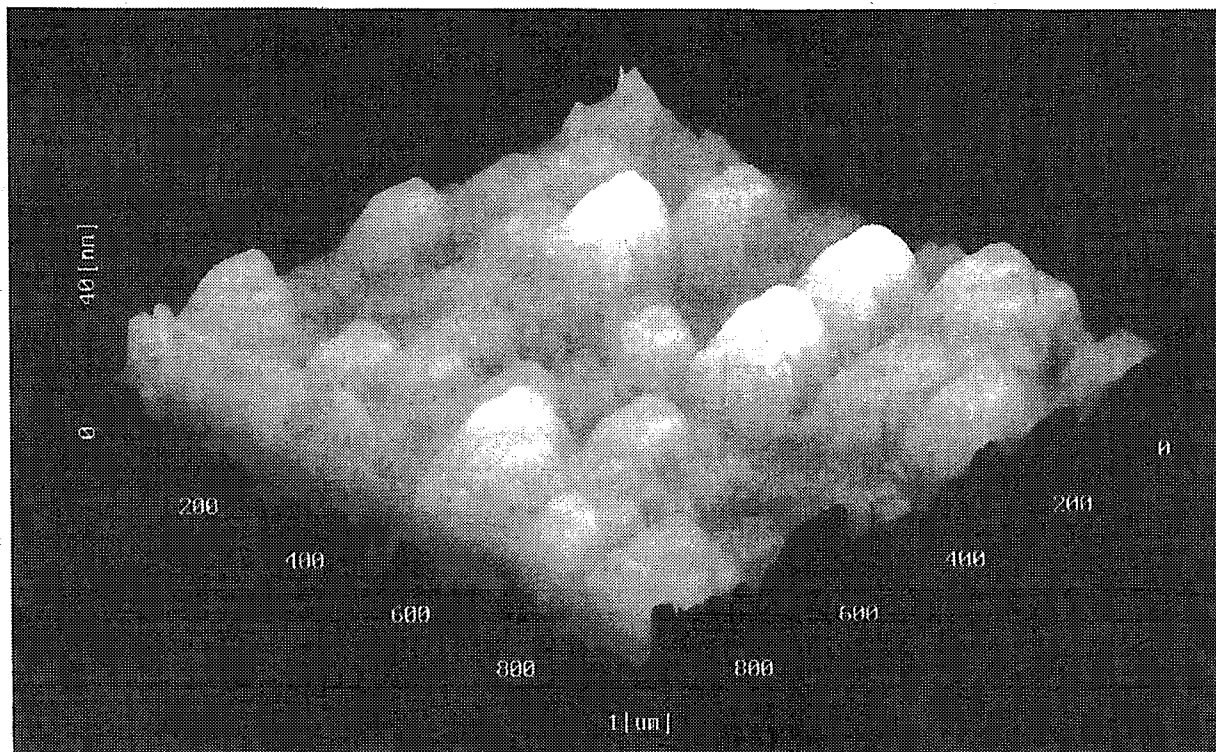
Figure 4.5b. Atomic force microscopy (AFM) image of carbon film obtained from camphoric carbon target.

4.4 Conclusions

In conclusion, we have investigated the characteristics of DLC films prepared by PLD from compressed camphoric carbon soot and conventional graphite targets. The films deposited from CC target are more diamond-like. The high deposition rate along with the better structural and optoelectronic properties demonstrated its usefulness as an alternative target to graphite for PLD. Camphoric carbon target can also be used in other physical deposition methods such as sputtering, FCVA, etc. for its practical implementation in tribology and semiconductor technologies. Furthermore, we would like to suggest the possibility of growing diamond films from camphor in modified conditions and/or using shorter wavelength lasers without additional hydrogen in contrast to graphite target. Also, other allotropes of carbon, such as, fullerenes, nanotubes etc. might be obtained by pulsed laser and other physical deposition methods using the CC targets.

References

[1] M. Maldei, D. C. Ingram (Eds.), Proceedings of the 13th European Photovoltaic Solar Energy Conference, Nice, France, October 23-27, 1995, p. 1258.

[2] A. P. Malshe, S. M. Kanetkar, S. B. Ogale, S. T. Kshirsagar, J. Appl. Phys. 68 (1990) 5648.

[3] B. Dischler , A. Bubenzer , P. Koidl, Appl. Phys. Lett. 42 (1983) 636.

[4] N. Savvides, B. Window, J. Vac. Sci. & Technol. A 3 (1985) 2386.

[5] H. Wang, M. R. Shen, Z. Y. Ning, C. Ye, C. B. Cao, H. Y. Dang, H. S. Zhu, Appl. Phys. Lett. 69 (1996) 1074.

[6] V. S. Veerasamy, G. A. J. Amartunga, J. S. Park, H. S. Mackenzie, W. I. Milne, IEEE Trans. On Electron Device 42 (1995) 577.

[7] J. A. Martin, L. Vazques, P. Bernard, F. Comin, S. Ferrer, Appl. Phys. Lett. 57 (1990) 1742.

[8] M. C. Polo, J. Cifre, G. Sanchez, R. Aguir, M. Varela, J. Esteve, Appl. Phys. Lett. 67 (1995) 485.

[9] D.S. Knight, W. B. White, J. Mater. Res. 4 (1989) 385.

[10] M. Hanabusa, K. Tsujihara, IEEE J. Sel. Top. Quantum Electron. 1 (1995) 848.

[11] S. M. Mominuzzaman, K. M. Krishna, T. Soga, T. Jimbo, M. Umeno, Jpn. J. Appl. Phys. 38 (1999) 658.

[12] N. H. Cho, K. M. Krishnan, D. K. Veirs, M. D. Rubin, C. B. Hopper, B. Bhushan, D. B. Bogy, J. Mater. Res. 5 (1990) 2543.

[13] S. M. Mominuzzaman, K. M. Krishna, T. Soga, T. Jimbo, M. Umeno, Carbon 38 (2000) 127.

[14] D. Beeman , J. Silverman, R. Lynds, M. R. Anderson, Phys. Rev. B 30 (1984) 870.

[15] R. O. Dillon, J. A. Woollam, V. Katkanant, Phys. Rev. B 29 (1984) 3482.

[16] A. W. P. Fung, A. M. Rao, K. Kuriyama, M. S. Dresselhaus, G. Dresselhaus, M. Endo, N. Shindo, J. Mater. Res. 8 (1993) 489.

[17] M. Yoshikawa, G. Katagiri, H. Ishida, A. Ishitani, T. Akamatsu, Appl. Phys. Lett. 52 (1988) 1639.

[18] A. A. Puretzky, D. B. Geohegan, G. E. Jellison Jr., M. M. Mcgibbon, in: H. A. Atwater, J. T. Dickinson, D. H. Lowndes, A. Polman (Eds.), Film Synthesis and Growth Using Energetic Beams, San Francisco, U.S.A., April 17-21, 1995, Materials Research Society Symposium Proceeding 388 (1995) 145.

[19] J. Tauc, Amorphous and Liquid Semiconductors, Plenum Press, London, New York, 1974.

[20] M. A. Tamor, J. A. Haire, C. H. Wu, K. C. Hass, Appl. Phys. Lett. 54 (1989) 123.

[21] J. Robertson, Advances In Physics 35 (1986) 318.

[22] D. Dasgupta, F. Demichelis, C. F. Pirri, A. Tagliaferro, Phys. Rev. B 43 (1991) 2131.

[23] S. R. V. Silva, G. A. J. Amartunga, Thin Solid Films 270 (1995) 194.

[24] A. Matsuda, T. Yamaoka, S. Wolff, M. Koyama, Y. Ymanishi, H. Kataoka, H. Matsuura, K. Tanaka, J. Appl. Phys. 60 (1986) 4025.

[25] M. Ouyang, H. Hiraoka, Materials Sci. & Engg. B39 (1996) 228.

[26] J. Bulir, M. Jelinek, V. Vorlicek, D. Chvostova, L. Soukup, J. Non-Cryst. Solids 188 (1995) 118.

[27] T. Matsui, M. Yadasaka, K. Imai, S. Yoshimura, in: D. Dreifus, A. Collins, K. Das, T. Humphreys, P. Pehrsson (Eds.), Diamond for Electronic Applications, Boston, U.S.A., November 27-December 1, 1995, Materials Research Society Symposium Proceeding 416 (1996) 229.

[28] Because of the presence of $C-C$, $C-H$, $C=O$ bonds in the structure the starting precursor camphor, whereas, graphite has only $C=C$ bonded carbons in its structure.

[29] Low and different rate of deposition on quartz and silicon substrates reflect the low energy of the species ablated from graphite target.

Chapter 5

Phosphorus Doping and Defect Studies of Carbon Films

5.1 Introduction

Carbon-based heterostructures on silicon have already been reported [1-6] and thereby demonstrates the potentiality of carbon materials in electronic devices. Unlike silicon, carbon has both σ and π states while silicon and other group IV semiconductors has only σ states. Since π states are more weakly bonded, they lie closer to the Fermi level (E_F) than the σ states. Therefore, filled π states form valence band edges while empty π^* states form conduction band edges, and these (π and π^*) states control the characteristics of gap states. Microstructure in carbon is complicated due to the presence of both σ and π states. However, undoped carbon is reported to be weakly p-type [7] and presence of the high density of intrinsic defects restricts its successful doping which is the main barrier for its application in various electronic devices. Effective doping can modify electronic properties, specially gap states, conductivity, etc. in semiconductor materials. Attempts have been made to dope carbon films using various elements [7-12]. Veerasamy et al. [7] reported n-type doping of highly tetrahedral carbon (ta-C) using solid phosphorus (P), while nitrogen (N) is the common dopant in carbon films with few exceptions [8-9]. However, P doping in relatively smaller gap DLC film with optical gap close to that of silicon which has scope in optoelectronic device applications, is not reported so far. P is the widely used n-type impurity in silicon [13] and is a possible alternative to N in carbon [14]. Electronic doping in carbon films using P target is yet to be realized by PLD using conventional

Furthermore, our effort to get P doped carbon film by XeCl excimer laser using graphite target was unsuccessful.

Graphite is commonly used as the target material for physical vapor deposition of DLC films systems, such as filtered cathodic vacuum arc (FCVA) [4], sputtering [15], PLD [16], etc. Recently, we have reported that camphoric carbon (CC) soot obtained from burning camphor ($C_{10}H_{16}O$), a natural source, is a better precursor material than graphite because the CC has hydrogen abundantly in its structure [17].

In this work, we have investigated the effect of P incorporation in DLC films by PLD using CC target. The doping mechanism and defect states are studied by Raman spectroscopy, optical gap, temperature dependence conductivity and ESR analyses of the undoped and P-doped films as a function of P content.

5.2   Experimental Details

DLC films were deposited on silicon and quartz substrates by excimer laser (NISSIN 10X, XeCl, $\lambda = 308$ nm, $\tau = 20$ nsec, repetition rate = 2 Hz, spot size = 5.5 mm^2), which is focused on the target at an incident angle of $45°$ to the target normal. The schematic of the PLD chamber is shown in Fig 4.1 (Chap. 4). The substrate was mounted parallel to the target at a distance of 45 mm. The films were deposited at room temperature at a base pressure of 10^{-6} Torr. The laser pulse energy was 150mJ on the window. Details of the chemical structure of the starting precursor camphor, the camphor burning system and the target preparation method have been described in chapter 3. In brief, camphor was burnt in a quartz tube and the soot deposited along the walls of the tube was collected, dried in the oven and pressed into pellets in order to use them as targets in PLD. In order to dope, the CC soot was mixed with varying amount of red phosphorus powder (1, 3, 5 and 7% by mass) and compressed into pellets.

Optical properties of the films were investigated by spectral transmittance and reflectance measurements. Electron-beam-evaporated gold electrodes were used in a gap cell

configuration for conductivity measurements for camphoric carbon (CC) films deposited on quartz substrates.

5.3 Results and Discussions

5.3.1 Phosphorus Content in the Film

The atomic % of P in the film was determined by X-ray photoelectron spectroscopic (XPS) analyses. The instrument used was SSX—100 XPS system of Surface Science Instruments utilizing AlKα (hv = 1486.6 eV) radiation, under high vacuum conditions of ~ 10^{-10} torr. The data was evaluated on the basis of empirical atomic sensitivity factors that were included in the present system software and was taken to be 1.29 for P 2p, relative to C 1s (= 1.00). Figure 5.1 shows XPS spectrum of the carbon film obtained from camphoric carbon soot target with 5% P. To visualize clearly, XPS spectra of the C 1s and P 2p regions for the same sample are shown in the insets of Fig. 5.1.
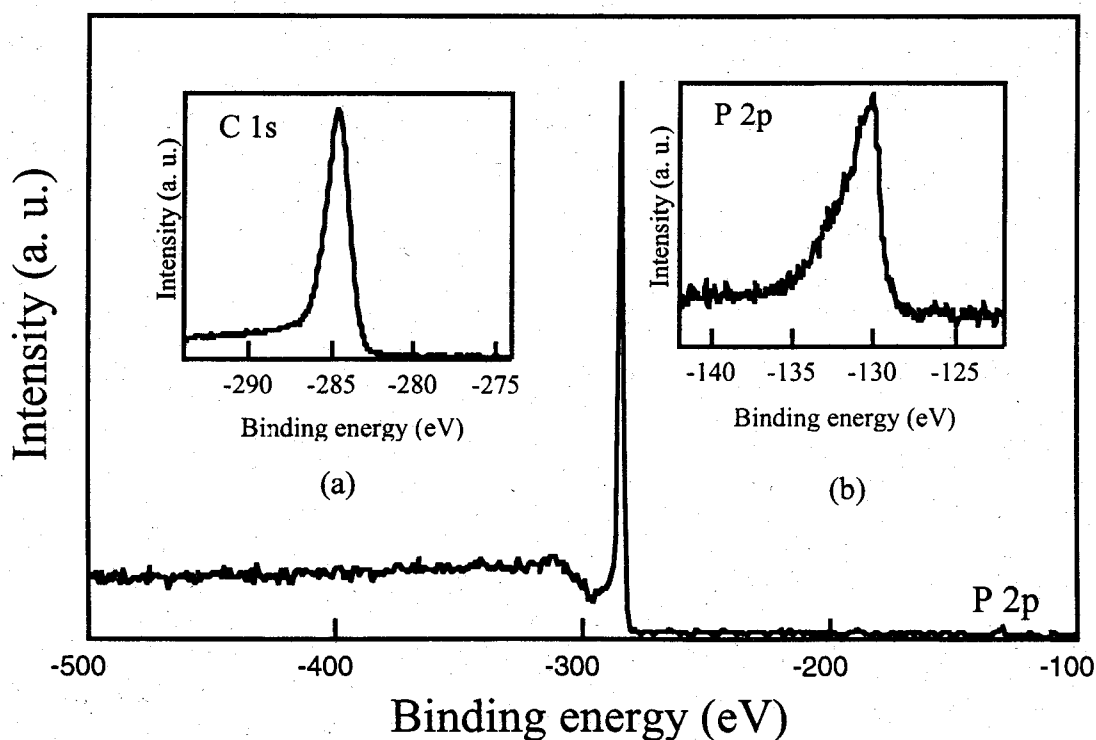
Figure 5.1. XPS spectrum of the carbon film obtained from camphoric carbon soot target with 5% P. Insets show XPS spectra of the a) C 1s region and (b) P 2p region for the same sample.

Figure 5.2 shows the variation of the atomic % of P in the carbon films as a function of P content by mass in the target. An approximately linear dependence of the atomic % of P in the film is observed with the P content in the target. The P content in the film increases from about 0.29 to 2 atomic % as the P content increases from 1 to 7% by mass in the target.
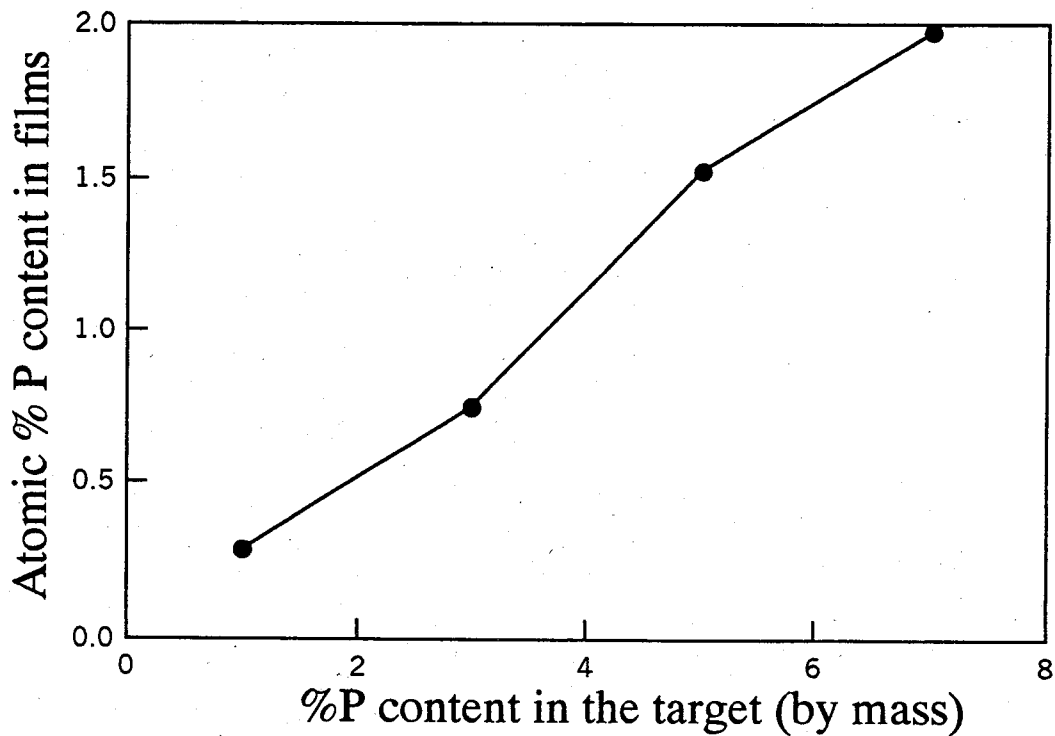
Figure 5.2. Variation of atomic P content in the carbon films as a function of P content by mass in the target.

5.3.2 Raman Spectroscopy

According to the theoretical model of Beeman et al. [18], the G line position is a measure of sp^2 fraction and is downshifted with increase of the sp^3 fraction in carbon films. The Raman spectra of undoped and P doped CC films are shown in Fig. 5.3. The experimental data are best fitted by two Gaussian lines and the G line position is about 1545 cm^{-1} for undoped CC film which remain almost same (in the inset of Fig. 5.3) even upon P addition. The shape and position of the spectra are almost unchanged. These results obtained from Raman analyses show that the structure of the films remain almost unaltered upon incorporation of P.
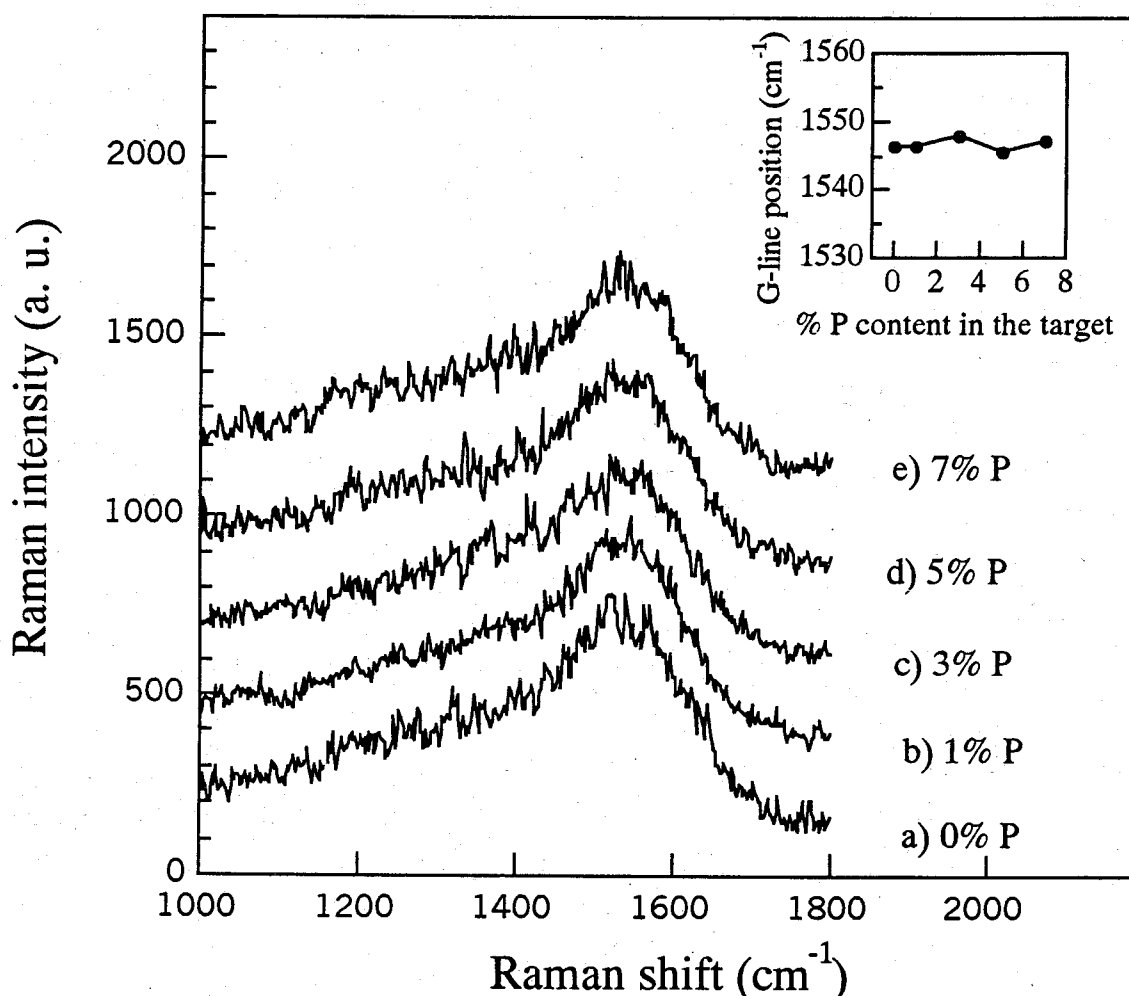
Figure 5.3. Raman spectra of the carbon films obtained from camphoric carbon soot targets with a) 0% P, b) 1% P c) 3% P d) 5% P and e) 7% P. The inset shows Raman G-line position of the same samples as a function of P content in the target.

5.3.3 Tauc Gap

From the measurements of optical reflectance and transmittance, optical absorption coefficient (α) is determined. The optical gap, E_{opt}, is obtained from the extrapolation of the linear part of the curve at the absorption coefficient $\alpha=0$ using the Tauc relation [19], $(\alpha h v)^{1/2} = B(E_{opt} - hv)$, where, B is the Tauc parameter. The estimated optical gap of undoped CC film is about 0.85eV which remains approximately unchanged for the films deposited using targets containing up to 5% P. However for the films deposited from the target containing 7% P, the gap decreases to 0.75eV as can be estimated from the Tauc plot in Fig. 5.4 for the undoped CC film and doped CC films deposited from targets containing 1% and 7% P.
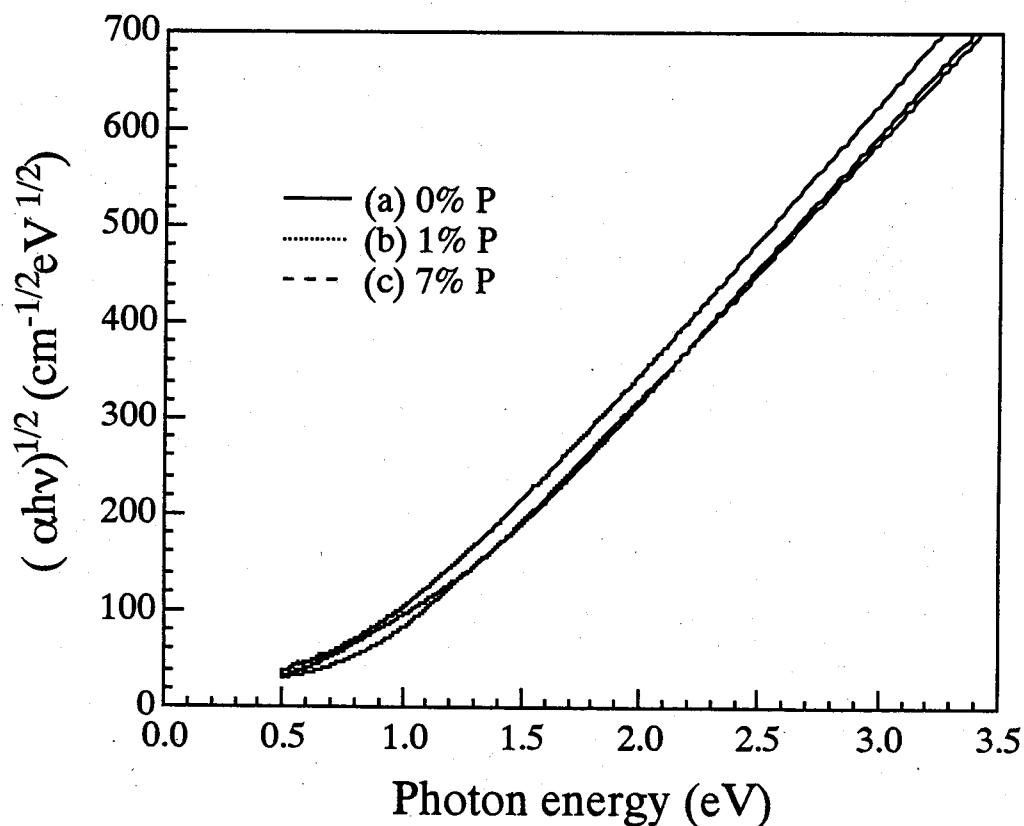
Figure 5.4. A plot of $(\alpha h v)^{1/2}$ as a function of photon energy (hv), for the carbon films obtained from camphoric carbon soot targets with a) 0% P, b) 1% P and c) 7% P.

The decline in optical gap for the film deposited from the target containing 7% P indicates increase of sp^2 fraction due to graphitization of CC film which is probably induced by high P content similar to the high N content induced graphitization [20] in nitrogen doped films.

5.3.4 Temperature Dependence Conductivity

The temperature (T) dependence of electrical conductivity (σ) is measured for undoped and P doped carbon films and is shown in Fig. 5.5, where conductivity is plotted against inverse temperature on a logarithmic scale. The conductivity of the film is seen to vary with P content in the target which decreases initially with addition of small amount of P (1%) and then increases sharply and gradually thereafter as the P content in the target increases to 7%.
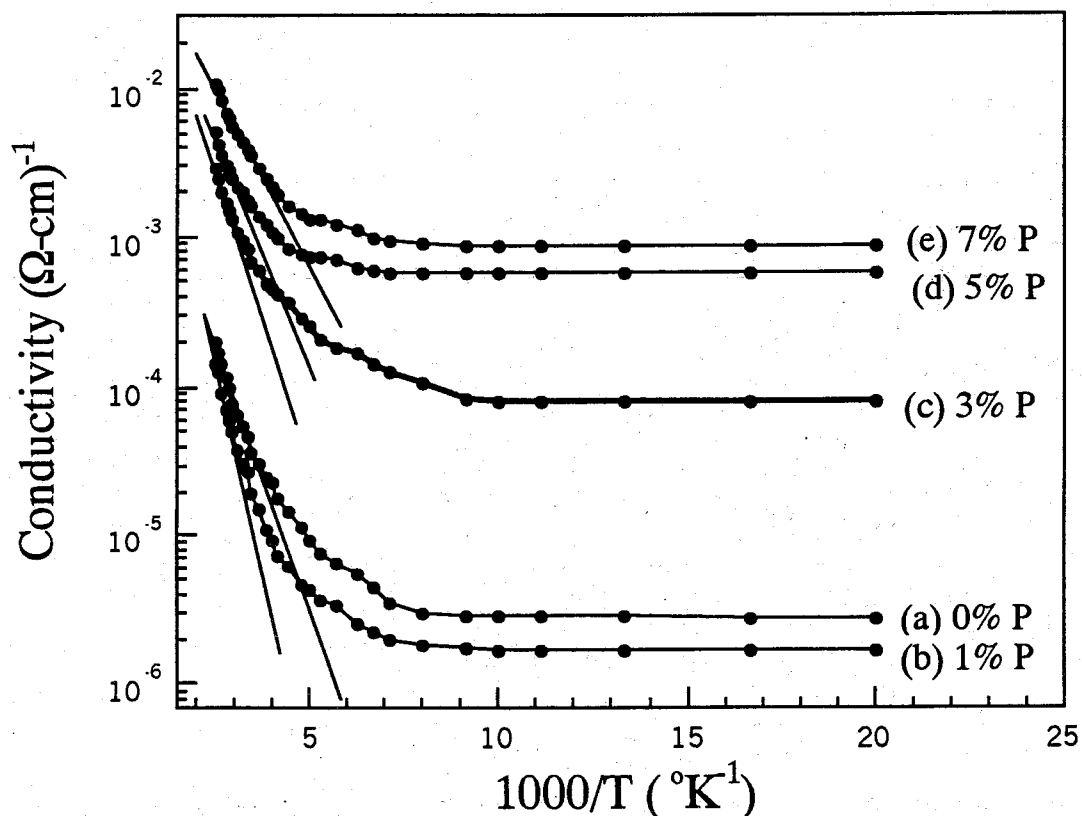
Figure 5.5. The temperature dependent conductivity of the carbon films obtained from camphoric carbon soot targets with a) 0% P, b) 1% P c) 3% P d) 5% P and e) 7% P.

5.3.5 Activation Energy and Room Temperature Conductivity

Above room temperature, the conduction mechanism is suggested to be in the extended states as ln σ versus 1/T is linear and the temperature at which the activation starts is observed to shift to lower value with P content. These results are similar to those reported by Veerasamy et al.[7]. Below room temperature, the slope of the ln σ versus 1/T plot changes and at further lower temperature, the increase of conductivity with temperature is very low. The conduction mechanism for below room temperature and lower temperature region can be attributed to conduction in band tail states and variable range hopping via deep states [18], respectively. Therefore, the activation energy, E_a, is determined from the slope of ln σ versus 1/T for above room temperature region. Figure 5.6 shows room temperature conductivity (σ_{RT}) and activation energy as a function of % P content in the target.
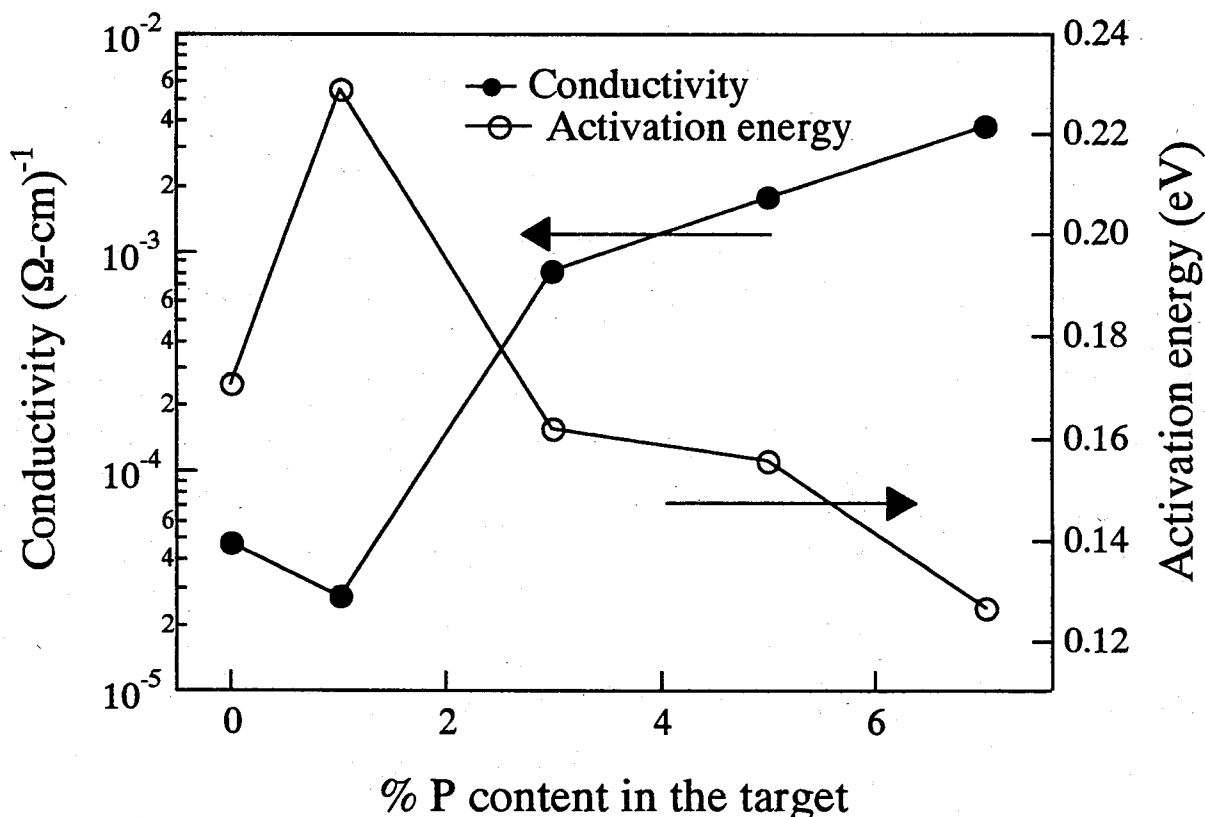
Figure 5.6. Variation of the room temperature conductivity and activation energy of the carbon films as a function of % P content in the target.

The E_a of undoped film is about 0.17eV and increases to about 0.23eV for the film deposited from target containing 1% P, whereas, σ_{RT} of undoped film is about 5×10^{-5} $(\Omega\text{-cm})^{-1}$ and decreased to 2.5×10^{-5} $(\Omega\text{-cm})^{-1}$ for the film deposited from target contains 1% P. With further increase of P content, the E_a decreases and conductivity increases sharply and gradually thereafter till they reaches the values of about 0.12eV and 3.8×10^{-3} $(\Omega\text{-cm})^{-1}$, respectively, as the P content in the target increased to 7%. The dependency of E_a and conductivity is different from that reported by Amaratunga et al. [10] where they found only decrease of E_a and increase of conductivity with P in their ta-C films.

5.3.6   Electron Spin Resonance Spectroscopy

Various defects which are related to electronic disorder, created due to different bonding configurations and give rise to the gap states around Fermi level (E_F), can be either paramagnetic or diamagnetic. The paramagnetic defects can be measured by ESR. The decrease of spin density is sharper at low concentration of P following a gradual decrease at higher concentration. This indicates that high density of defects in undoped CC film restricts the doping. Upon compensation/passivation of defects at low concentration of P incorporation (1%), doping efficiency increases.

The variation of ESR spin density and ESR linewidth of the films as a function of % P content in the target are shown in Fig. 5.7. The spin density is seen to decrease with P content, whereas ESR linewidth increases with P content for the films deposited from target containing up to 5% P and decreases thereupon. Our results are similar to Bhattacharyya et al.[21] where they have reported decrease of the spin density and increase of the ESR linewidth with increasing N content. However, they have observed gradual decrease of optical gap with N content, whereas, optical gap is seen to remain unaltered for the CC films deposited from target containing up to 5% P.
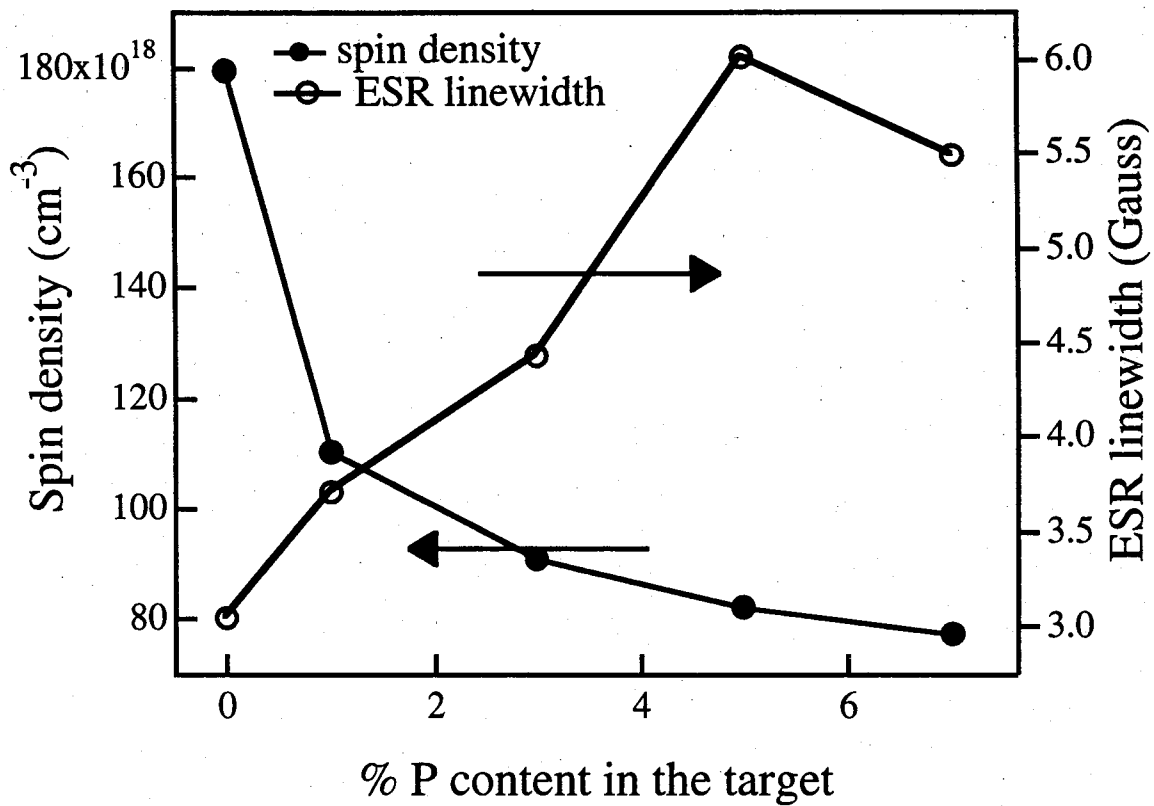
Figure 5.7. Variation of the ESR spin density and ESR linewidth of the carbon films as a function

of % P content in the target.

5.3.7 Doping Mechanism

The decrease of spin density is sharper for the film deposited from the target containing 1% P following a gradual decrease with the increase of P content (Fig. 5.7). This indicates presence of defect states restricts doping initially. Undoped DLC is lightly p-type due to the presence of acceptor like defect states and small amount of P addition compensates/passivates the acceptor like defect states by the ionized electrons from P atoms. Therefore, conductivity is observed to decrease while activation energy is observed to increase as E_F moves through the mid gap for the film deposited from the target containing 1% P (Fig. 5.6). With further increase of P content, Fermi level moves towards conduction band edge and activation energy decreases while the conductivity increases.

5.3.8 Phosphorus as n-Type Impurity in Carbon

We have measured I-V characteristics of the undoped carbon film on n type silicon and P incorporated carbon film on p type silicon. When a negative bias was supplied to the substrate of the former, the junction was forward biased while for the latter, the junction was forward biased with reverse polarity suggesting p-type nature of the undoped carbon and n-type nature of the P incorporated carbon film. Details of the junction characteristics that vary systematically with P content in the carbon film will be presented in the next chapter. As the optical gap is observed to decrease only little for the film deposited from target containing 7% P, we speculate that both P induced graphitization and doping are responsible for increase of the conductivity. ESR linewidth is increased (Fig. 5.7) possibly due to the gradual loss of homogeneous spin environment [22] with P addition. However, for the film deposited from the target containing 7% P, the decrease of ESR linewidth could be related to the graphitization of carbon network.

5.4 Conclusions

Phosphorous is doped in carbon films using camphoric carbon soot target by pulsed laser deposition technique. The electrical properties and defect states are studied. Study of activation energy suggests that the Fermi level of the carbon film is moved from valence band edge to near to the conduction band edge through mid gap. The variation of conductivity is in good agreement with the activation energy analyses. As optical gap remains almost constant, successful doping is realized for the films deposited from the target containing up to 5% P. The decrease of ESR spin density reveals modifications of the gap states with increase of P content.

References

[1] N. Konofaos, C. B. Thomas, Appl. Phys. Lett. 61 (1992) 2805.

[2] M. Maldei, D. C. Ingram, in; Proc. 13th European Photovoltaic Solar Energy Conference, Nice, 1995, p. 1258.

[3] F. J. Clough, W. I. Milne, B. Kleinsorge, J. Robertson, G. A. J. Robertson, B. N. Roy, Electron Lett. 32 (1996) 498.

[4] V. S. Veerasamy, G. A. J. Amartunga, J. S. Park, H. S. Mackenzie, W. I. Milne, IEEE Trans. on Electron Device 42 (1995) 577.

[5] K. M. Krishna, S. M. Mominuzzaman, N. Inada, T. Soga, T. Jimbo, M. Umeno, in: Proc. 2nd World Conf. on Photovoltaic Solar Energy Conversion, Vienna, 1998, p. 164.

[6] H. A. Yu, T. Kaneko T, S. Yoshimura, Y. Suhng, S. Otani, Y. Sasaki, Appl Phys Lett 69 (1996) 4078.

[7] V. S. Veerasamy, G. A. J. Amaratunga, C. A. Davis, A. E. Timbs, W. I. Milne, D. R. Mackenzie, J. Phys.: Condens. Matter 5 (1993) L169.

[8] D. I. Jones, A. D. Stewart, Philos. Mag. B 46 (1982) 423.

[9] M. Alaluf, L. Klibanov, N. Croitoru, Diamond Relat. Mater. 5 (1996) 1497.

[10] G. A. J. Amaratunga, V. S. Veerasamy, C. A. Davis, W. I. Milne, D. R. Mackenzie, J. Yuan, M. Weiler, J. Non-Cryst. Solids 164-166 (1993) 1119.

[11] D. Chen, A. Wei, S. P. Wong, S. Peng, Diamond Relat. Mater. 8 (1999) 1130.

[12] L. K. Cheah, X. Shi, J. R. Shi, E. J. Liu, S. R. P. Silva, J. Non-Cryst. Solids 242 (1998) 40.

[13] K. Kadas, G. G. Ferenczy, S. Kugler, J. Non-Cryst. Solids 227-230 (1998) 367.

[14] M-T. Kuo, P. W. May, A. Gunn, M. N. R. Ashfold, R. K. Wild, Diamond Relat. Mater. 9 (2000) 1222.

[15] S. M. Mominuzzaman, K. M. Krishna, T. Soga, T. Jimbo, M. Umeno, Carbon 38 (2000) 127.

[16] M. C. Polo, J. Cifre, G. Sanchez, R. Aguir, M. Varela, J. Esteve, Appl. Phys. Lett. 67 (1995) 485.

[17] S. M. Mominuzzaman, T. Soga, T. Jimbo, M. Umeno, Thin Solid Films, 376 (376) 1.

[18] D. Beeman , J. Silverman, R. Lynds, M. R. Anderson, Phys. Rev. B 30 (1984) 870..

[19] J. Tauc, R. Grigorovici, A. Vancu, Phys. Status Solidi 15 (1966) 627.

[20] S. R. P. Silva, J. Robertson, G. A. J. Amaratunga, B. rafferty, L. M. Brown, J. Schwan, D.F. Franceschini, G. Mariotto, J. Appl. Phys. 81 (1997) 2626.

[21] S. Bhattacharyya, C. Vallee, C. Cardinaud, O. Chauvet, G. Turban, J. Appl. Phys. 85 (1999) 2162.

[22] N. Fourches, G. Turban, Thin Solid Films 240 (1994) 28.